The Critical Role of Asphaltene Nanoaggregates in Stabilizing Functionalized Graphene in Crude Oil Derivatives

(article starts on next page)

The critical role of asphaltene nanoaggregates in stabilizing functionalized graphene in crude oil derivatives

Govindan Induchoodan [a,b,*], Helen Jansson [b], Amir Saeid Mohammadi [c], Jan Swenson [a]
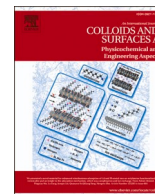
[a] *Department of Physics, Division of Nano & Biophysics, Chalmers University of Technology, SE 412 96 Göteborg, Sweden*
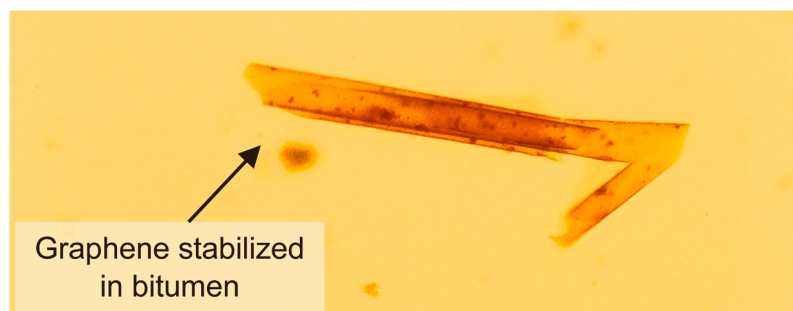[b] *Department of Architecture and Civil engineering, Division of Building Materials, University of Technology, SE 412 96 Göteborg, Sweden*
[c] *Department of Architecture and Civil engineering, Division of Water & Environment Technology, Chalmers University of Technology, SE 412 96 Göteborg, Sweden*

HIGHLIGHTS

- First successful method to stabilize graphene derivatives in bitumen.
- Solution to overcome adsorption of asphaltene aggregates on graphene derivatives.
- Asphaltene nanoaggregates and resins used to stabilize graphene derivatives.
- Toxic-free, environment-friendly solution with ability to improve the properties of bitumen.

GRAPHICAL ABSTRACT

Graphene stabilized in bitumen

ABSTRACT

Graphene derivatives have been seen as an additive to improve the material properties of bitumen, such as thermal conductivity, viscoelasticity, and mechanical strength. However, in our previous work, a critical challenge was identified. When graphene derivatives are incorporated into bitumen, it leads to detrimental effects. This is due to the poor phase compatibility of graphene derivatives with asphaltene aggregates, the intrinsic aggregates that give bitumen its characteristic properties. In this work, we focus on tailoring the surface chemistry of graphene, thorough non-covalent functionalization, to achieve phase compatibility with asphaltene aggregates. In addition, the work also focuses on stabilizing this functionalized graphene in bitumen. To achieve this, the graphene was functionalized with -COOH tethers by the Molecular wedging method. Thereafter, the same molecules that form the asphaltene aggregates were used to stabilize the functionalized graphene by embedding the -COOH tethers in the asphaltene aggregates. As a result, graphene functionalized by this strategy was observed to be stable in bitumen and phase compatible with asphaltene aggregates. Thus, a successful environment-friendly strategy was developed to utilize the potential of graphene to improve the material properties of bitumen.

Keywords:
Non-covalent functionalization
Graphene
1-pyrene butyric acid
Molecular wedging
Asphaltene aggregates
XPS
SAXS
DSC

1. Introduction

Bitumen, a crude oil derivative, is a highly viscous colloid that consists of four molecular fractions of molecules [1–3]. These are saturates, aromatics, resins, and asphaltenes, which together are called SARA fractions [1–3]. The most important molecular group amongst this is asphaltenes due to their influence on the structure and function of bitumen [2–11]. Asphaltenes are complex poly-aromatic hydrocarbons that form the solid fraction of bitumen. While they are highly studied, the definite structure of asphaltenes is still debated [5–11]. However, these molecules are inferred to have an average size of 7 aromatic rings, with a nearly 50% structural ratio of aromatic to alicyclic and open-chain aliphatic [11].

In bitumen, asphaltenes are often predicted to be in a low-energy state. The low-energy state of asphaltenes is called the asphaltene nanoaggregates [10,11]. The asphaltene nanoaggregates are formed through the mutual interaction of the asphaltenes [10,11]. They have an approximate size of 2 nm, i.e., less than 10 stacked molecules, see Table 1. Thereafter, the four molecular fractions in bitumen interact to form non-isodiametric aggregates, called asphaltene aggregates [1–3, 12]. These structures are formed when asphaltene nanoaggregates interact with resins. Resins are semi-solid and less polar than asphaltenes and act as surfactants in bitumen [2,3,12–17]. As a surfactant, tails of resins in an asphaltene aggregate extend into the surrounding saturates and stabilize asphaltene aggregates. In addition, these tails contribute to steric stabilization and interaction between the asphaltene aggregates [1–3,12–17]. These asphaltene aggregates give bitumen its colloidal structure [10]. Moreover, the asphaltene aggregates can mutually interact to form larger cluster structures over time [10,11]. In this study, the clustered structure is called a ''network structure''.

Due to its colloidal structure, bitumen has poor thermal conductivity [1]. Furthermore, its complex molecular structure makes it highly susceptible to weather (e.g., temperature and moisture change) and can undergo heavy structural damage due to cyclic loading [1–3,10]. To augment the material properties of bitumen and improve durability, nanoparticles, such as graphene derivatives, have been suggested as an excellent additive [18–31]. This is due to their desirable properties, such as extremely high thermal conductivity and mechanical strength. However, as shown in our previous study, incorporating graphene derivatives into bitumen can cause the asphaltene aggregates to irreversibly adsorb onto the graphitic surface [32]. Thus, negatively impacting the colloidal structure and the function of bitumen. Furthermore, the adsorption occurs due to i). hydrogen bonding between the graphene derivatives and asphaltene nanoaggregates [33], ii). acid-base interactions between the graphene derivatives with oxygenated groups, such as graphene oxide (GO) and the heteroatomic functional groups on resin and the asphaltene nanoaggregate [33–37], and iii). π-π interactions between the polyaromatic structures of the asphaltene nanoaggregates and the hexagonal carbon structure of graphene derivatives [33–36]. After the irreversible adsorption, all the solid phases in bitumen precipitate. Thus, it was evident that graphene derivatives (such as GO) are detrimental to the asphaltene aggregates and, thereby, the properties of bitumen [32]. Therefore, their interaction must be modified to overcome the structural instability of asphaltene aggregates due to the graphene derivatives (such as GO), and instead, form a phase-compatible structure with each other that will contribute to the properties of bitumen. The potential strategy to achieve such a phase-compatible structure is discussed in this work.

To develop such a phase-compatible structure in bitumen, in this study, graphene was functionalized by the Molecular wedging method, in which 1-pyrene butyric acid (1-PBA) was non-covalently attached to the graphene surface [38–46]. See Table 2 for an illustration and definition of the graphene structure and the overview of the terminologies for different states/length scales of the functionalization. The butyric acid groups (hereafter called the -COOH tethers) attached on the surface are expected to interact with the heteroatoms on asphaltene

nanoaggregates and resins. Following this interaction, the asphaltenes and resins will form asphaltene aggregates at the -COOH tethers, see Table 1. This form of asphaltene aggregates, with -COOH tethers embedded in them, are called tethered asphaltene aggregates. This novel hybrid structure in which the tethered asphaltene aggregates stabilize the PBA-graphene is called the PBA-graphene ensemble. The PBA-graphene used in this study is produced by non-covalent functionalization. This functionalization strategy will retain the sp2 hybridized state of graphene to a large extent [38–46]. Graphene is highly thermally and electrically conductive due to its sp2 hybridized state [38–46]. Thus, maintaining the sp2 hybridized implies that PBA-graphene is expected to retain many material properties from the pristine graphene while being able to interact with molecules in bitumen (unlike pristine graphene, which is inert) [38–46].

The PBA-graphene ensemble developed in this study is predicted to be stabilized by the tethered asphaltene aggregates. Thus, the tethered asphaltene aggregates (on the PBA-graphene ensemble) are expected to behave like the ordinary asphaltene aggregates in bitumen. The stability of the asphaltene aggregates is a highly studied subject [47–74], and it has been shown that asphaltene aggregates precipitate in crude oil/-bitumen with increased concentrations of short-chain alkane like n-hexane [2,3,47–68]. In the presence of n-hexane, the tails of resins (on the asphaltene aggregates) will condense, causing a reduction of its steric stability. This, in turn, affects the stability of the asphaltene aggregates. As the concentration of n-hexane is increased, these tails will eventually collapse onto the asphaltene aggregates resulting in flocculation and precipitation [69–73]; see Fig. 1. The tethered asphaltene aggregates on the.

PBA-graphene ensemble, developed in this study, is expected to behave similarly in the presence of n-hexane.

Various models, such as the Flora Huggins parameter [74], the solubility parameter [75], and the Coil-Globule transition [76], have been used to explain the process leading to flocculation and precipitation. In addition, numerous experimental techniques, such as microscopy, spectroscopy, rheometry, and titration studies, have also been used to investigate the precipitation of asphaltene aggregates [74]. However, the precise mechanism of the induced precipitation kinetics in the presence of n-alkanes is not well understood. Nevertheless, it has been concluded that the precipitation behavior depends on factors such as the solvent, solvent-aggregate interaction kinetics, viscosity of the system, observation time, temperature, and type of asphaltene nanoaggregates [2–4,47–57,68–74]. By comparing the stability of the PBA-graphene ensemble with the asphaltene aggregates in the presence of n-hexane, it is possible to investigate the influence of the tethered asphaltene aggregates on the stability of the PBA-graphene ensemble [74].
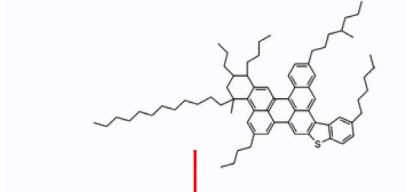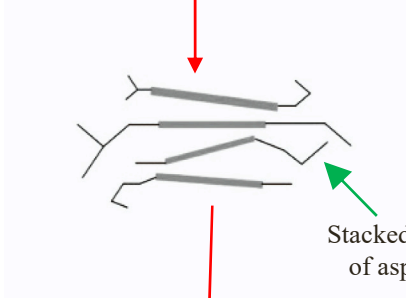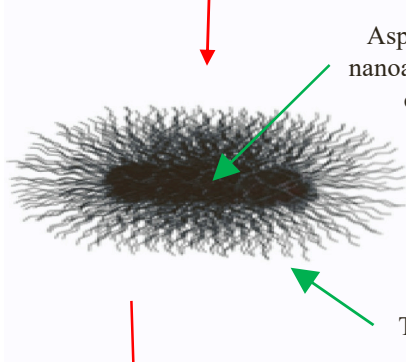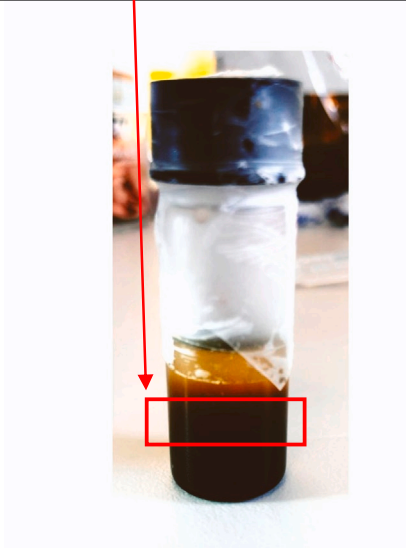
This implies that this study focuses on:

1. The development of a novel hybrid colloidal structure of the PBA-graphene ensemble.
2. The influence of tethered asphaltene aggregates on the stability of the PBA-graphene ensemble.
3. A solution to overcome the detrimental effects observed by the introduction of graphene derivatives (such as GO) in bitumen [32].
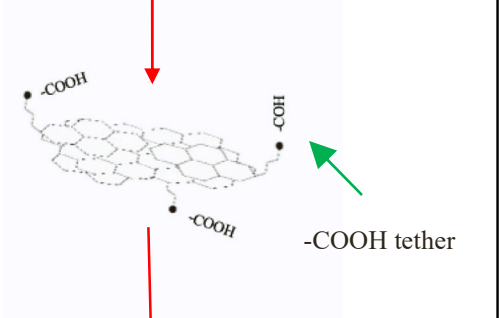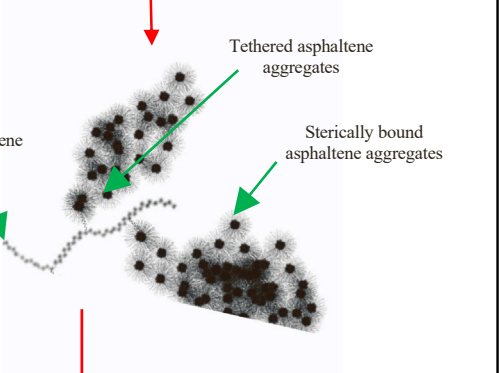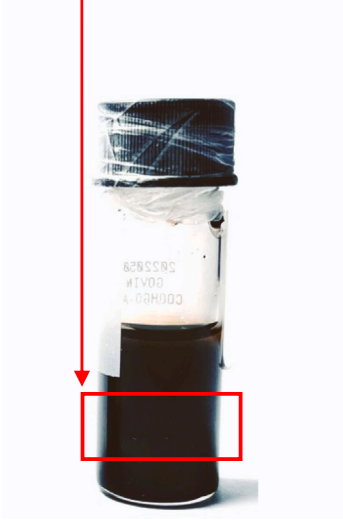
In this study, a simplified representation of bitumen called the asphaltene aggregate system is used [32]; refer to Table 1. It has a fixed volume of asphaltene nanoaggregates, surfactants, and saturates. The fixed volume of the molecular groups helps study the interaction of the PBA-graphene and the asphaltene aggregates more accurately. Unlike the asphaltene aggregate system, in bitumen, the volume fractions of the 4 molecular groups can vary due to many internal and external factors. Further, the surfactant 4-dodecylbenzene sulfonic acid (DBSA) was used instead of resins to stabilize the asphaltene nanoaggregates [47–57]. DBSA has an alkyl aryl sulfonate head and a 12-carbon tail [47–57]. The simple chemical structure and high efficiency of DBSA in stabilizing asphaltene aggregates in bitumen, have made DBSA a popular surfactant

Table 1
Description of the states of asphaltene used in this study and the illustrations of the corresponding structures.

Sample	Definition	Illustration
Asphaltene	Molecular state of the asphaltene (1 molecule).	
Asphaltene nanoaggregate	Low energy state of asphaltene, when extracted from crude oil (less than 10 stacked asphaltenes)	Stacked structure of asphaltene
Asphaltene aggregate	Stable aggregates of asphaltene nanoaggregates in the saturates, formed with the use of surfactants such as resins or DBSA.	Asphaltene nanoaggregate core Tails of resins
Asphaltene aggregate system	A simplified model system used in this study. It contains asphaltene aggregates dispersed in saturates [32].	

Table 2

Description of the states of graphene used in this study and the illustrations of the corresponding structures.

Sample	Definition	Illustration
Graphene	The graphene that was received from the supplier	
PBA-graphene	Graphene that was functionalized using the Molecular wedging method and has -COOH tethers on the surface.	-COOH tether
PBA-graphene ensemble	Novel hybrid structure with PBA-graphene (core) that has tethered asphaltene aggregates attached to it via the -COOH tethers and is stable in saturates	Tethered asphaltene aggregates; PBA-graphene; Sterically bound asphaltene aggregates
PBA-graphene system	A simplified model system used in this study and is equivalent to PBA-graphene incorporated bitumen. It contains the PBA-graphene ensemble and all possible structures formed by the interaction between the different chemical constituents used to develop the system.	
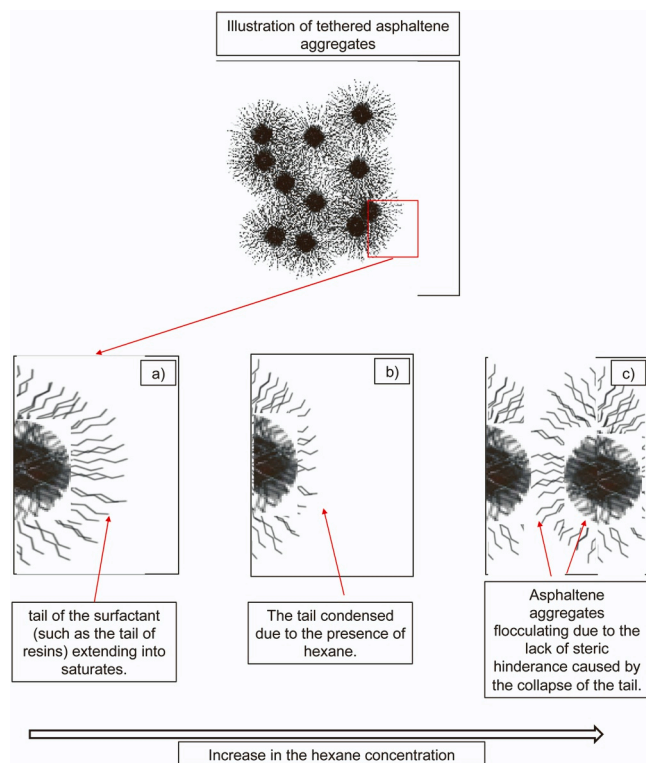
Fig. 1. A schematic illustration of the collapse of the dodecyl tail of DBSA on the asphaltene aggregate. a). The stable asphaltene aggregate in saturates. b) With the introduction of a precipitant such as n-hexane, the stability of the asphaltene aggregates is reduced. c). With further increase in the n-hexane concentration the tail of surfactant (such as the tail of resins) collapse and the asphaltene aggregates start to agglomerate, which in turn leads to flocculation. This eventually leads to the precipitation of the asphaltene aggregates in the system.

and a replacement for resins, (which are known to be chemically complex) [47]. Thus, DBSA is widely utilized as a surfactant for asphaltene nanoaggregates both in industry and academia [47–57]. Lastly, the system studied in this work that comprises of the PBA-graphene ensemble (and all possible structures formed by the interaction between the chemical constituents, i.e., PBA-graphene, asphaltene nanoaggregates and DBSA, in saturates) is called the PBA-graphene system, see Table 2. The PBA-graphene system is a simplified representation of a PBA-graphene incorporated bitumen, similar to how the asphaltene aggregate system is a simplified representation of bitumen.

Finally, to investigate the structure, structure development and stability of the model systems, several instrumental techniques, such as dynamic light scattering (DLS), small angle X-ray scattering (SAXS), transmission light spectroscopy, and rheology were used. From the results, it is concluded that the structure and stability are dependent on the number of the -COOH tethers available on the surface of the PBA-graphene and that the shape of graphene (dot, ribbon, sheet), and the number of functionalized sites (-COOH tethers) determine the final shape of each PBA-graphene ensemble. Furthermore, both the asphaltene aggregates and the PBA-graphene ensemble are stabilized by the dodecyl tails of the DBSA. In addition, the results show that both the asphaltene aggregate system and the PBA-graphene system display a similar behavior with increasing temperature, flow, and in the presence of short-chain alkane. Thus, by non-covalently functionalizing graphene, by the Molecular wedging method, the detrimental effect of graphene derivatives on bitumen is overcome; and a phase compatible graphene was developed.

2. Materials

Graphene (M-grade XGnP) was purchased from XGScience. The 'as received' nanoplatelets (graphene), has a surface area of 120–160 $m^2 g^{-1}$, a thickness of 6–8 nm, a density of 2.2 $kgcm^{-3}$, and a diameter of 25 μm. The supplied XGnP has an oxygen and residual sulfur content of less than 1 and 0.5 elemental%, respectively [77]. The asphaltene nanoaggregates were extracted from the bitumen supplied by Skanska AB (Sweden), for more details see elsewhere [32]. DBSA, analytical grades n-heptane (99.9%), n-hexane (99.9%), toluene (90%), ethanol (99%) and 1-PBA, were purchased from Sigma Aldrich. The 60 R Group I Baseoil was obtained from Chevron and was used as the saturates.
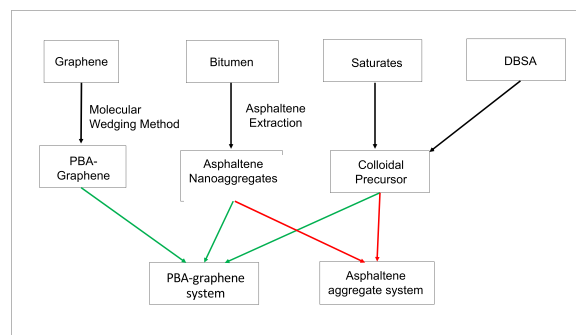
2.1. Preparation of the asphaltene aggregate system

Before extracting the asphaltene nanoaggregates from bitumen, the asphaltene content in bitumen was increased by the rolling thin-film oven test setup (RTFOT) [78]. The extraction of asphaltene nano-aggregates was performed according to the American Society for Testing and Materials (ASTM) D-2007–80 standard [79]. As a first step, n-heptane was added in a ratio of 100 ml to 1 g of bitumen and placed in a flask, in a silicon oil bath, on a heating/magnetic steering plate. A Dimroth reflux condenser, connected to a water supply with appropriate pressure, was placed on top of the flask and then the entire setup was sealed using clamp. The solution was then heated to 95 °C and steered for 1 h before it was turned off. The solution was thereafter poured into 30 ml conical centrifuge tubes and centrifuged at 4000 rpm for 5 min using a Sigma 4–16 centrifuge. Finally, the solution was decanted, and the precipitate was air-dried for 24 h to ensure that the extracted material was completely dry of any solvent.

Thereafter, a colloidal precursor was prepared by dispersing 0.5 ml of DBSA in 10 ml of saturates (≈ 5 wt%). First, 5 mg of the extracted asphaltene nanoaggregates was dispersed in 1 ml of toluene. This dispersant was sonicated, centrifuged, and air-dried to remove any residual solvents under reduced pressure. The asphaltene aggregate system used for the experiments was prepared by dispersing 5 mg of asphaltene nanoaggregates in 5 ml of the colloidal precursor, and vigorously shaken. Then sonicated for 15 min prior to the measurements. See Fig. 2 and Table 3 for a more detailed description of the involved steps and weight fractions used for the sample preparation.

2.2. Preparation of PBA-graphene

Graphene was functionalized by the Molecular wedging method

Fig. 2. : A flow chart of the sample preparation of the asphaltene aggregate system and the PBA-graphene system. As shown in the figure, the PBA-graphene was synthesized from graphene, and asphaltene nanoaggregates were extracted from bitumen. The colloidal precursor was prepared from DBSA and saturates. The asphaltene aggregate system was prepared by dispersing the asphaltene nanoaggregates in the colloidal precursor and the PBA-graphene system was prepared by dispersing the PBA-graphene and the asphaltene nanoaggregates in the colloidal precursor.

Table 3

Weight fractions (wt%) of the different components used to produce the asphaltene aggregate system and the PBA-graphene system.

Name	Saturates (wt%)	DBSA (wt%)	Asphaltene nanoaggrgates (wt %)	PBA-graphene (wt%)
Colloidal Precrusor	95	5	-	-
Asphaltene aggregate system	90	5	5	-
PBA-graphene system	89	5	5	1

[38–46]. Accordingly, 100 mg of graphene was dispersed in 50 ml methanol and sonicated for one hour to disperse the graphene flakes; following that, 16.5 mg of 1-PBA was added to the solution, and it was further sonicated for an hour. After this, 200 ml of double-distilled de-ionized water was added, and the solution was sonicated for 24 h at room temperature and thereafter centrifuged. Subsequently, the precipitate was decanted and redispersed in de-ionized water. The redispersed solution was further sonicated for 45 min, filtered, and rinsed. This process was repeated 3 times. The material was thereafter vacuum-dried at 60 °C to remove any residual water.

The functionalized PBA-graphene was inspected for dispersibility and stability in water, as described in S1 of the supplementary information (SI). Graphene is not dispersible in water, but, on the other hand, the graphene functionalized with 1-PBA (COOH group) should be water-soluble because COOH is water-miscible. The PBA-graphene and non-functionalized graphene were both visually inspected after dispersing in water, for 24 h, and it was confirmed that PBA-graphene was water dispersible, which provided a visual confirmation of the functionalization (see Fig. S1 of SI).

2.3. Preparation of the PBA-graphene system

1 mg of the prepared PBA-graphene was dispersed in 10 ml methanol and sonicated for 45 min in a water bath at a constant temperature of 20 °C. The solution was thereafter centrifuged at 4500 rpm for 5 min and decanted. This was repeated twice, and thereafter air-dried. To prepare the PBA-graphene system, a volume fraction of 10 wt% PBA-graphene was introduced into the asphaltene aggerate system and sonicated for 10 min. A description of the involved steps and weight fractions of the prepared PBA-graphene system is shown in Fig. 2 and Table 3, respectively.

2.4. X-ray photoelectron spectroscopy

To verify and characterize the adsorption of 1-PBA on the surface of graphene, the PBA-graphene was measured by a PHI5000 VersaProbe III- Scanning XPS microprobe. For the measurements a monochromatic Al source with an energy of 1486 eV and a beam size of 100 μm was applied. Since the PBA-graphene is expected to be non-conductive, a dual charge compensation of an argon ion gun (+ve) and an electron neutralizer (-ve) were used. Au4f7/2 (83.96 eV), Ag3d5/2 (368.2 eV) and Cu2p3/2 (932.6 eV) were used to align the XPS. The alignment was performed by measuring the sp2-hybridized carbon in graphene at 284.5 eV. Narrow scans were performed to study the chemical state of carbon and oxygen. The measurements were performed with a step size of 1.0 eV. For a reference to the XPS spectra of asphaltene nano-aggregates and DBSA, see our previous work [32].

2.5. Differential scanning calorimetry

The measurements were carried out by use of a TA Instrument DSC Q2000. A Standard heating scans (5 °C/min) of both the asphaltene aggregate system and the PBA-graphene system were performed in the temperature range − 100 – 125 °C. The samples were placed in hermetically sealed pans. Each sample was measured 3 times to ensure repeatability. The specific temperatures and temperature ranges for the different thermal events occurring during heating were determined using Universal Analysis (UA) software.

2.6. Small angle X-ray scattering

The SAXS measurements were performed using a SAXSLAB Mat: Nordic, manufactured by SAXSLAB / Xenocs. Both the asphaltene aggregate system and the PBA-graphene system were diluted at a rate of 1:10 (in saturates). Separate samples were prepared at a n-hexane concentration of 0%, 1%, 5%, 10%, 25%, and 50%. Following this, the samples were rested for 24 hrs and thereafter transferred to 1.5 mm diameter capillary tubes. Before the measurements, the instrument was aligned by using silver behenate. Each sample was measured for 600 s. The measurements were performed with a sample-detector distance of ~1084 mm, which gives, a q-range of 0.005–0.25 Å^{-1}, which corresponds to the range of 125–2.5 nm in real space. Further, a beam size of 0.3 mm was used. Finally, a sample of saturates was measured. The scattering intensity of the saturates was subtracted from all samples before comparing. For this, the scattering intensity of saturates was first multiped with 0.99 (0.99 represents the total concentration of saturates in both asphaltene aggregate system and PBA-ensemble system after dilution for the SAXS measurements), and following the multiplication, the scattering intensity at the corresponding q value was subtracted from the sample.

2.7. Transmission bright field microscopy

The structure and structural development of the PBA-graphene ensemble in bitumen was monitored by the use of an Olympus BX53 microscope. A drop of the sample was placed on a glass slide for each measurement. The measurements were performed in the transmission mode at ambient conditions, with at magnifications of 2X, 10X, 20X, and 40X.

2.8. Experimental flowcharts

A summary of the sample preparation procedures is shown in Fig. 2 as a flowchart. It provides a concise view of the different steps involved in the development of the asphaltene aggregate system and the PBA-graphene system from the initial materials, i.e., bitumen and graphene. Table 3 presents the individual constituents used to prepare the asphaltene aggregate system and the PBA-graphene system (in wt%). Table S1 of SI provides an overview of the experimental techniques used in this study and the expected information of each used technique.

3. Results and discussion

In order to verify the functionalization and the structure of the PBA-graphene measurements were performed using XPS and Raman spectroscopy. XPS was used to verify the attachment of 1-PBA onto graphene, and Raman spectroscopy was used to verify the exfoliation of graphene during molecular wedging. Microscopy was used to investigate the structure and structural development of the PBA-graphene ensemble. DLS and SAXS were used to study the influence of the tethered asphaltene aggregates on the stability of the PBA-graphene ensemble. In addition, rheology was applied to both systems to understand the viscosity effect of incorporating PBA-graphene. Finally, DSC was used to evaluate the thermal stability of both systems.

3.1. Verification of the synthesis of the PBA-graphene

XPS scans were performed to investigate and verify the expected

functionalization by the Molecular wedging method. As shown in Fig. 3, the results obtained by XPS show that there is nearly 21 elemental% of oxygen in PBA-graphene. The oxygen is in the form of oxygenated carbon species. The graphene provided by the supplier contains < 1 elemental% of oxygen [77], and therefore is a clear indication that the synthesis has substantially increased the concentration of oxygen. Further, the scans provide C1s oxygenated carbon peaks between 283 eV and 288 eV (Fig. 3a), and O1s oxygenated carbon peaks between 530 eV and 536 eV (Fig. 3b).

In the C1s spectra, the peak at 287.1 eV indicates the presence of C=O, and the peaks at 286.2 eV and 285.4 eV indicate the existence of C-O and C-OH, respectively (Fig. 3a). The occurrence of the C=O peak, together with the C-OH peak, gives an indication of carboxylic acid (C(=O)(OH)) [80]. The C1s scan also shows the presence of a C-C peak at
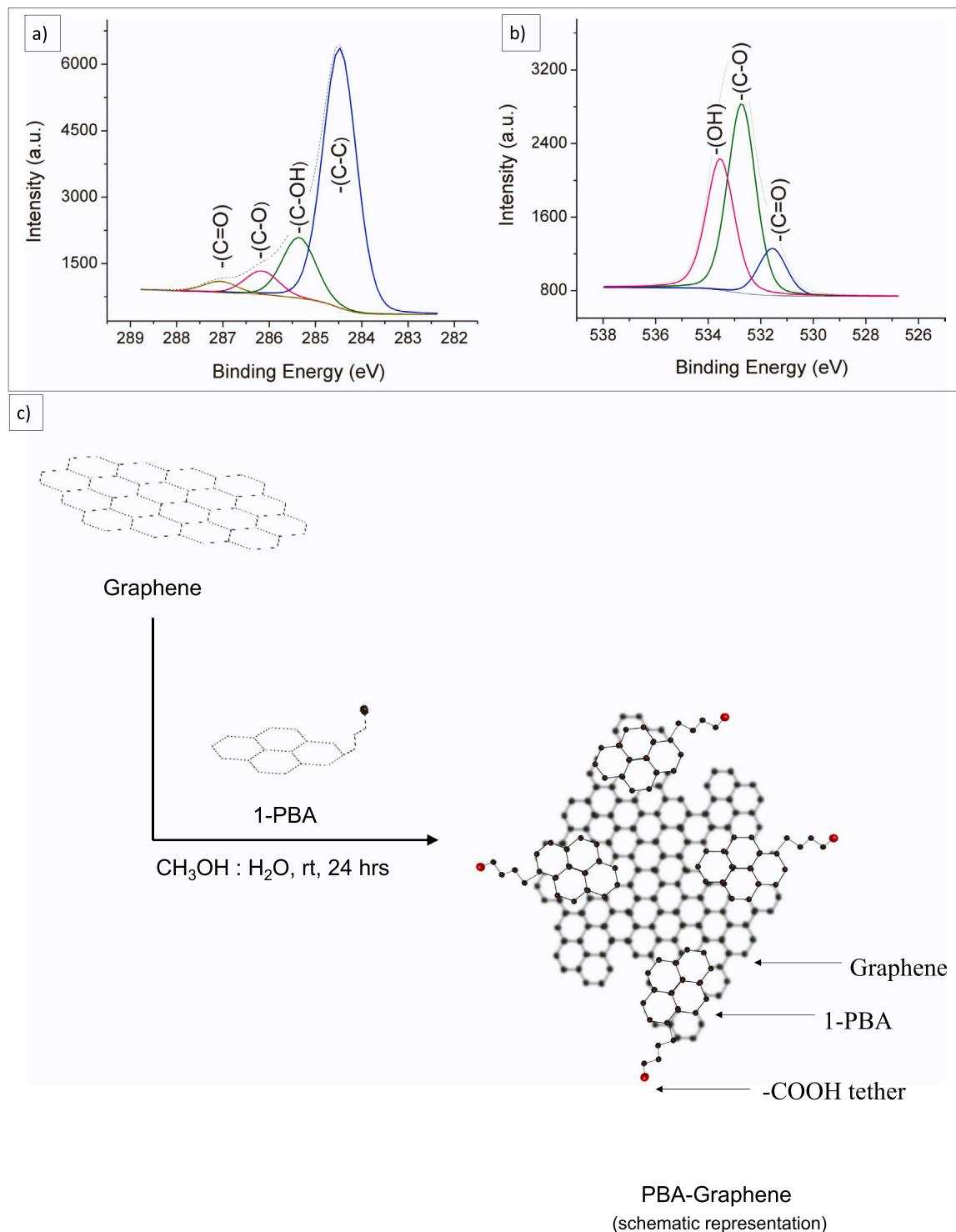
Fig. 3. : C1s and O1s XPS spectra of the PBA-graphene. The overall scans indicate that there is 78.6 elemental% of carbon and 21.4 elemental% of oxygen in the PBA-graphene. a). and b). show the C1s and O1s spectra of oxygenated carbon species, respectively, which confirms the attachment of -COOH groups on the graphene surface. This observation thus verifies the functionalization of graphene by the Molecular wedging method. In c). a schematic of the predicted structure of the non-covalently functionalised PBA-graphene is provided.

284.5 eV, which is from the graphitic surface. In the O1s spectra (Fig. 3b), there is a peak at 533.5 eV showing the presence of the -OH group, which arises from the -COOH group. In the O1s spectra, there are also peaks from C-O and C═O, at 532.7 eV and 531.6 eV, respectively. Both C1s and O1s spectra give evidence of the attached carboxylic acid. From the XPS data, it is thus evident that the synthesis by use of the Molecular wedging method was successful and that the 1-PBA was attached to graphene.

The exfoliation of graphene by the Molecular wedging method is further verified by Raman spectroscopy; see Fig. S2 of SI. The shift in the position and the intensity of the G band (in-plane breathing vibration) indicates a reduction in the number of layers of the graphitic structure after molecular wedging, see Fig. S2 of SI. Additionally, the formation of the molecular defects on the edges (increase in the intensity of the D band, out-of-plane vibration) of the graphene further support the successful exfoliation by the Molecular wedging method. From a combination of visual inspection, XPS, and Raman spectroscopy, it is thus evident that the synthesis by the Molecular wedging method, was successful. From the XPS and Raman results, the structure and structural development of the PBA-graphene ensemble can be predicted; an illustration is displayed in Fig. 3c.

As described in the introduction, the asphaltene nanoaggregates and DBSA introduced to the PBA-graphene system will form tethered asphaltene aggregates at the -COOH tethers. The sulfonic acid on DBSA will, in turn, interact with the functional groups of the asphaltene nanoaggregates to form a stable structure. This is because sulfonic acids are more acidic than carboxylic acids, and in the presence of DBSA, the -COOH tethers will act as a base [47–57]. This will causes an acid-base reaction that will bind the DBSA to the -COOH tether on PBA-graphene.

3.2. Observation of the structure of the PBA-graphene ensemble

The structure prediction from the XPS results is verified by transmission bright-field microscopy of the PBA-graphene system, see Fig. 4. As can be observed, there is a large structure, i.e., the PBA-graphene ensemble, surrounded by the saturates. The PBA-graphene ensemble is seen to have a PBA-graphene with dark dots (tethered asphaltene aggregates) randomly distributed all across its surface.

To further understand the structure of the PBA-graphene ensemble and its structural evolution over time, the PBA-graphene ensemble was studied over a week after the sample preparation. The results are shown in Fig. 5, where 5a-c shows the structure formation and development at 2, 3, and 7 days, respectively. This series of images shows how the asphaltene aggregates form a network structure around the PBA-graphene ensemble. By comparing the results obtained at 2 days (Fig. 5a) with those at 3 or 7 days (Figs. 5b or 5c), it is clear that the network structure is growing more prominent with time. The formation and growth of the network structure is due to the tethered asphaltene aggregates, interacting with other asphaltene aggregates formed outside the PBA-graphene (called untethered asphaltene aggregates). Thus, the formation of the network is due to the interaction between the untethered and tethered asphaltene aggregates.

It is well known that functional groups on the asphaltene nanoaggregates are critical for the formation of asphaltene aggregates [2–4, 33–37,47–78]. Therefore, the stability of the PBA-graphene ensemble (Figs. 4–6) is obtained by the formation of the tethered asphaltene aggregates attached to the -COOH tethers on the PBA-graphene. The -COOH tethers on the PBA-graphene can therefore be considered to act as the initiation or nucleation sites to form the PBA-graphene ensemble, as illustrated in Fig. 6. Furthermore, as shown in Fig. S3 of SI, the PBA-graphene ensemble can contain various shapes and surface features, like creases, protrusions, tears, and folds, which clearly indicate that the growth of the asphaltene aggregate formation at the -COOH tethers is independent of the shape of the PBA-graphene itself. Therefore, the stability and formation of the PBA-graphene ensemble can be attributed to the number of -COOH tethers on the surface of the
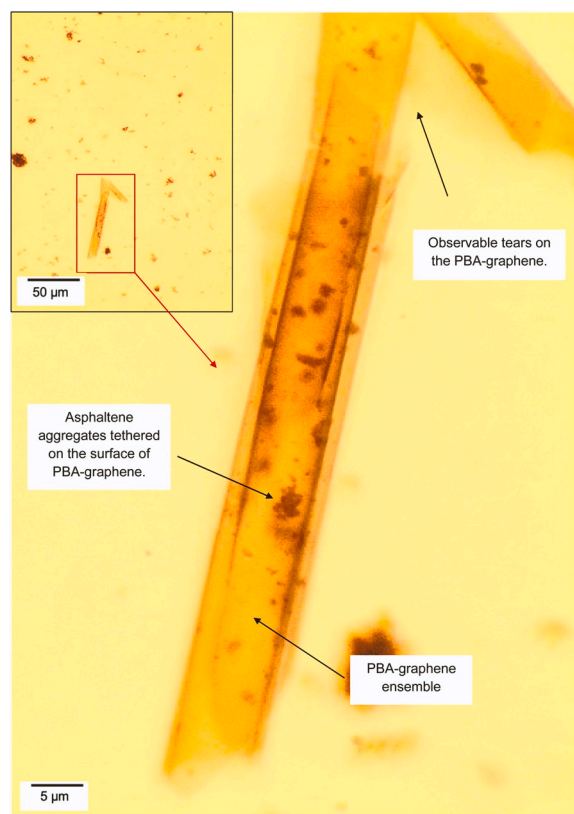

Fig. 4. : Transmission bright field image of the PBA-graphene ensemble in saturates. From the image it is shown that the structure of the PBA-graphene is twisted inwards. Asphaltene aggregates are seen as dark dots on the surface. Inset: Zoomed out image of the PBA-graphene ensemble.
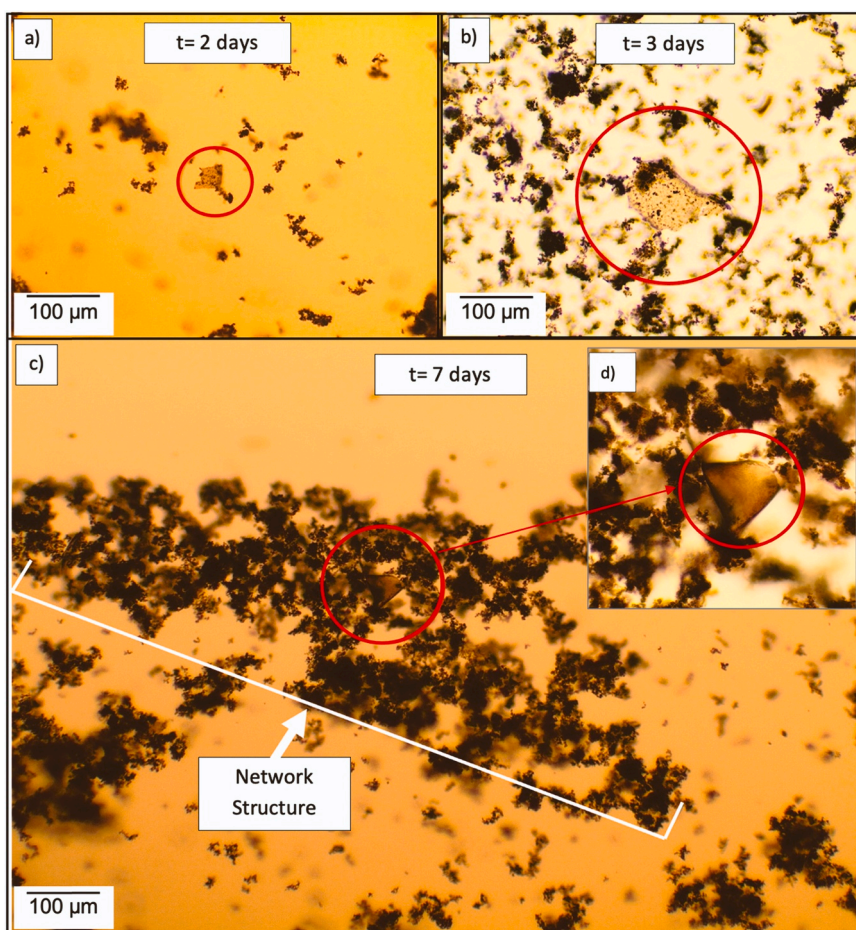
PBA-graphene.

3.3. Influence of the tethered asphaltene aggregates on the stability of the PBA-graphene ensemble

To investigate the role of the tethered asphaltene aggregates in stabilizing the PBA-graphene ensemble and identify the similarity in stability of the asphaltene aggregate system and the PBA-graphene system, both systems were investigated in the presence of a precipitation agent by SAXS and DLS (S.I.) and at elevated temperatures using DSC. Firstly, to prove the importance of asphaltene nanoaggregates for the stability of the PBA-graphene ensemble, a sample was prepared without asphaltene nanoaggregates and visually observed. The conditions at which the sample was prepared for visual observation of the system without asphaltene nanoaggregate is presented in section S4 of SI. As shown in Fig. S4 of SI, in the absence of the asphaltene nanoaggregates, DBSA bound PBA-graphene lacks stability in saturates. This implies that the PBA-graphene ensemble does not form a self-stabilizing structure in saturates. Instead, it confirms that the formation of tethered asphaltene nanoaggregates is essential to stabilize PBA-graphene in bitumen.

Following the visual observation, SAXS was performed to identify the influence of n-hexane on the stability of the two systems studied in this work. Fig. 7 shows the scattering intensity at the momentum transfer q= 0.005 Å⁻¹ with increasing n-hexane content. This q-value corresponds to a length in real space of around 125 nm. At this length scale, the observed scattering intensity arises from large structures such as the PBA-graphene ensemble, tethered asphaltene aggregates, and untethered asphaltene aggregates in the PBA-graphene system. In the asphaltene aggregate system, the intensity is due to suspended asphaltene aggregates.

The results from the SAXS measurements indicate that we have

Fig. 5. : Transmission bright field image of the PBA-graphene ensemble (marked with a red circle) at a) t = 2 days, b) t = 3 days, and c) t = 7 days. Over time, it is obvious that the network formation, which consists of sterically bound asphaltene aggregates, around the PBA-graphene ensemble is growing. In figure d). a zoomed in image of the PBA-graphene of the PBA-graphene ensemble displayed in (c) is shown.

different effects of adding n-hexane, depending on the concentration. In the concentration range 0–1%, the interactions between the structures in both systems appear to dominate. This leads to a growth of larger structural aggregates i.e., flocculation up to 1% of n-hexane. For the PBA-graphene system, there is a substantial decrease in scattering intensity (see Fig. 7). The dominating effect seems to be that structural aggregates of a size approximately corresponding to the given q-value, i. e., 125 nm, flocculate to larger clusters, which would only be observed if the SAXS instrument could measure lower q-values. This interpretation is consistent with results from DLS measurements (table S2 of SI), which show that at 1% n-hexane the average size of the aggregates has grown considerably. In the case of the asphaltene aggregate system, the structural aggregates are smaller on average, and therefore the dominating effect when 1% hexane is added is that aggregates smaller than 125 nm flocculate to larger aggregates, which contribute to the scattering intensity at the given q-value. This is likely the reason for why the same type of flocculation, as occurring for the PBA-graphene system, in this case increases the scattering intensity, see Fig. 7.

In the concentration range of 1–10% n-hexane, the intensity increases for the PBA-graphene ensemble, as shown in Fig. 7, which likely is because smaller aggregates, as for the asphaltene aggregate system, have flocculated to a size of about 125 nm, thereby contributing to the observed scattering intensity at the given q-value. Thus, the flocculation can both increase and decrease the scattering intensity at the q-value depending on whether the aggregates grow to a size corresponding to the detected length scale or to a size that is too large to be observed by the instrument. Furthermore, sufficiently large aggregates are expected

to precipitate in this concentration range. The combined effect of these phenomena causes a moderate increase in the scattering intensity of the PBA-graphene system. Conversely, for asphaltene aggregates, the increase in n-hexane concentration leads to a decrease in scattering intensity followed by a moderate increase in scattering intensity, similar to the PBA-graphene system. The contributing effect of precipitation is also visually evident. As seen in Fig. 7 (asphaltene aggregate system at 10% n-hexane), the top of the cuvette is lightly colored, while lower down, the sample is darker colored (indicating the onset of precipitation).

Beyond 10% n-hexane, the scattering intensity decreases mainly due to precipitation. This is indicated by the SAXS data shown in Figs. S5a and S5b of S.I., which shows that the scattering intensity also decreases at higher q-values due to the reduction of aggregates of all sizes. This precipitation is also visually evident from the images of the prepared samples. Both samples show a visual lightning of color, indicating precipitation. However, at 50% n-hexane concentration, the asphaltene aggregate system shows a more considerable decrease in the scattering intensity compared to the PBA-graphene system. This is also evident in the visual observation of the cuvettes in which the asphaltene aggregate system shows higher precipitation compared to the PBA-graphene system.

Furthermore, the SAXS measurements show that both systems display a similar response to the introduction of n-hexane. Thus, it seems very likely that both systems have identical stabilization mechanisms. Since it is well established that the dodecyl tails of DBSA stabilize asphaltene aggregates, the results suggest that in the PBA-graphene system, the PBA-graphene ensembles are also stabilized by the
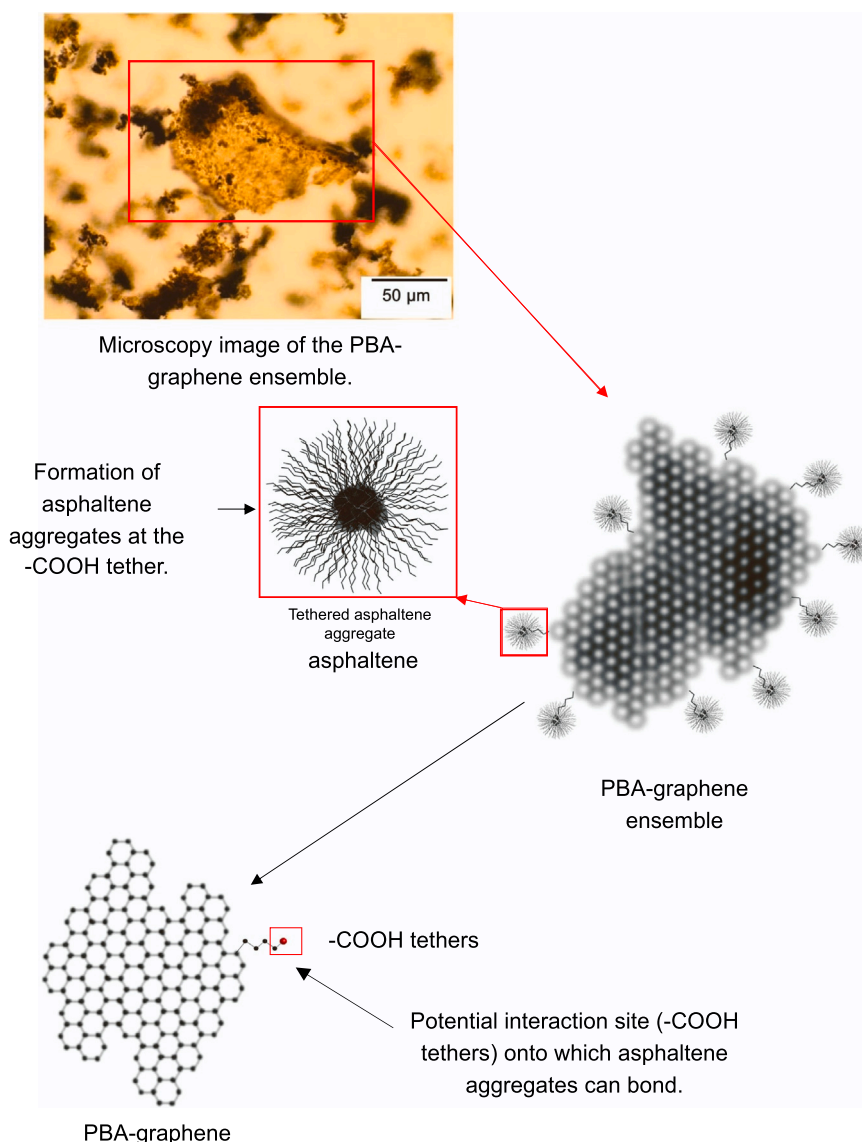
Fig. 6. Schematic structure of the PBA-graphene ensemble based on the microscopic image shown in the top of the figure, i.e., the PBA-graphene with the asphaltene aggregates formed at the -COOH tethers. It should be noted that the structure of the asphaltene aggregates illustrated in the figure is only for an illustrative purpose.

dodecyl tails of DBSA in the tethered asphaltene aggregates. DLS further supports this conclusion. As can be seen in table S2 of S.I., with increasing n-hexane concentration, both systems show a similar shift in the hydrodynamic diameter. Due to the polydispersity and polymorph nature of both systems, it should, however, be noted that the hydrodynamic diameters presented in S.I. are only average values of very broad distributions of aggregate sizes, as discussed above in the interpretation of the SAXS data.

This understanding about the similarity between both systems is further confirmed through the results from DSC measurements, see Fig. 8. The results show that both the asphaltene aggregate system and the PBA-graphene system display a similar thermal response. For both the asphaltene aggregate system and the PBA-graphene system there is a broad glass transition (T_g) around $-80\,°C$. The origin of the broadness gives an indication on that there may be two glass transitions close to each other, which previously has been suggested [81]. Previous studies on similar systems, as well as bitumen, have shown that this low temperature T_g is due to an onset of molecular rearrangements in the saturates [82,83]. In addition, for both samples, there is an exothermal event with a peak maximum around $-25\,°C$ that is due to cold crystallization of the waxy part of the saturates [84]. At higher temperatures

there is an indication of a very broad glass transition for both the asphaltene aggregate system and the PBA-graphene system. However, due to the risk of evaporation of the saturates, which gives a limitation in measuring the samples at higher temperatures, this cannot be verified.

The similarity in the DSC curves of the asphaltene aggregate system (upper curve) and the PBA-graphene system (lower curve) implies that the PBA-graphene ensembles will behave in the same way as the asphaltene aggregates during heating. Thus, the general understanding of the behavior of the asphaltene aggregates in bitumen (and its consequent impact on roads) can be extrapolated to a potential bitumen design based on the PBA-graphene ensemble. Therefore, it can be concluded through SAXS, DLS, and DSC that both systems are stabilized by similar mechanism. This is important since the PBA-graphene ensemble must thus be stable at thermal conditions in which bitumen is used. For instance, bitumen is used as the surface layer of roads, and thereby exposed to diurnal and seasonal temperature variations, typically between $-20\,°C$ and $50\,°C$. Further, during processing and transportation, bitumen is in general heated up to relatively high temperatures (close to $130\,°C$). Therefore, it is important that the thermal stability of the PBA-graphene ensemble is similar as for the asphaltene aggregates in bitumen.
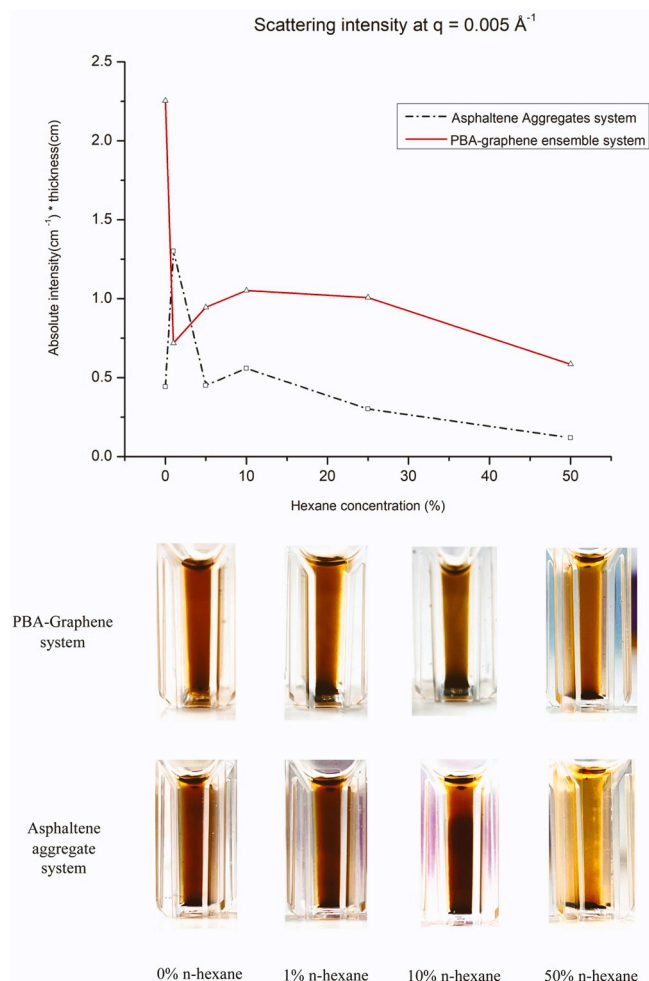
Fig. 7. : The scattering intensity of the asphaltene aggregate system and PBA-graphene system at a q-value of 0.005 Å⁻¹ measured using SAXS. The data points represents the drop in scattering intensity with increase in n-hexane concentration. The scattering intensity of saturates was subtracted from all the samples. Below the graph, the images of the samples prepared with different n-hexane concentrations at each zone is presented.
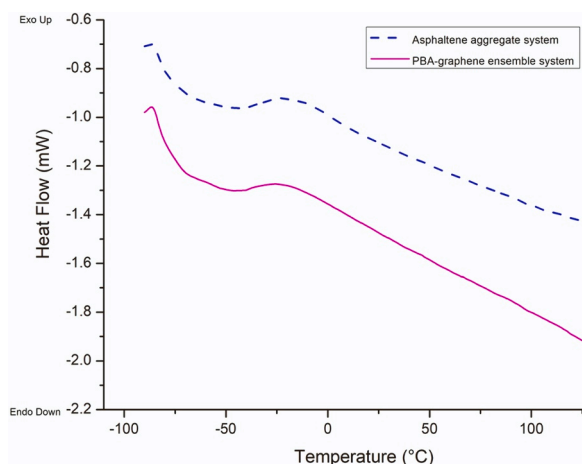
Fig. 8. : DSC heating curves of the asphaltene aggregate system (upper curve) and the PBA-graphene system (lower curve).

3.4. Future areas of applications of the PBA-graphene ensemble

Asphalt is made of stones (called 'aggregate' by the road engineering industry, called 'stones' here to differentiate from 'asphaltene aggregate') and bitumen (the binder) [1]. It is known that the asphaltene aggregates cluster around the stones [1]. This implies that the PBA-graphene ensemble and the extensive network structure will also be located around the stones, thereby forming a large solid phase around it. Therefore, the potential of the PBA-graphene ensemble to locate itself around the stones can be utilized to tailor the microstructure of asphalt, for instance, to increase the thermal conductivity.

In cold countries, up to a million tons of salt are used annually to maintain ice-free roads during the winter [84], which often ends up in the ecosystem along the roads and results in environmental issues. Due to this, de-icing by heating the roads is seen as an alternative, but the efficiency of this alternative solution is drastically limited by the low thermal conductivity of bitumen. A proposed solution to this problem is to incorporate graphene into bitumen to improve the thermal conductivity. The in-plane thermal conductivity of graphene of about 2000–4000 W·m^{-1}·K^{-1} is amongst the highest of any material [85]. This is attributed to the sp2 hybridized bond in the honeycomb structure [85]. During covalent functionalization, a large amount of the surface is transformed from an sp2 hybridized state to an sp3 hybridized state. On the contrary, with non-covalent functionalization (by the Molecular wedging method), a larger amount of the graphene surface is maintained in its sp2 hybridized state, thus maintaining the desired high thermal conductivity. Further, since the synthesis of the PBA-graphene is also environmentally friendly, if graphene has to be used to improve the thermal conductivity of bitumen, perhaps PBA-graphene can be a potential future solution.

Finally, the viscosity effect of incorporating the PBA-graphene is presented in Fig. S6 of S.I. The measurements show that the presence of PBA-graphene causes a substantial increase in the rest viscosity of the PBA-graphene system compared to the asphaltene aggregate system (an increase from 19.2 mPa-s to 33.5 mPa-s. The increase in the rest viscosity is due to the polymorphic nature of PBA-graphene and the network structure formed around the PBA-graphene ensemble. While the rest viscosity is high, when shear is increased, the viscosity drops to 24.2 mPa-s. The drop in viscosity is associated with the alignment of the PBA-graphene in the flow direction. Thus, incorporating PBA-graphene has a nominal effect on the viscosity. Further, since the structure of PBA-graphene can be tailored, its corresponding PBA-graphene ensemble can also have tailored structures. This implies that the PBA-graphene ensemble can be used to tailor the viscosity, viscoelastic, and through it, mechanical properties of bitumen. This, too, can have potential future applications; for example, it can be beneficial to use PBA-graphene to tailor the nanoparticles to contribute only to a minimum to the viscosity and the plasticity component of the viscoelasticity while improving the elastic component of bitumen. This can be achieved by utilizing the PBA-graphene ensemble to form controlled network structures that influence the behavior of bitumen.

4. Conclusion

This study focused on developing and characterizing the novel hybrid structure called the PBA-graphene ensemble, consisting of a PBA-graphene and the tethered asphaltene aggregates. The PBA-graphene is developed by functionalizing graphene using the Molecular wedging method. After which, asphaltene aggregates are used to stabilize the PBA-graphene and the subsequent formation of the PBA-graphene ensemble. The PBA-graphene ensemble is dispersible in saturates and phase compatible with asphaltene aggregates. The asphaltene nano-aggregates are identified to be critical in the formation and stabilization of the PBA-graphene ensemble in saturates.

The PBA-graphene system and the asphaltene aggregate system display similar stabilization mechanisms and thermal responses. These

characteristics give an indication that the production of bitumen with incorporated PBA-graphene will be similar to the production of conventional bitumen. Thus, no other industrial processes have to be developed to incorporate the PBA-graphene or lay roads with the PBA-graphene ensemble modified bitumen. Moreover, due to the simplicity of the functionalization and stabilization of PBA-graphene, the developed PBA-graphene system is not only cost-effective but also an environmentally conscious and effective method for the incorporation of a graphene derivative into bitumen.

CRediT authorship contribution statement

Govindan Induchoodan: Conceptualization, Methodology, Validation, Writing – original draft. **Helen Jansson:** Supervision, Validation, Writing – original draft. **Amir Saeid Mohammadi:** Researcher, Lab support, Experimental Work, Validation. **Jan Swenson:** Supervisor, Validation, Writing – original draft.

Declaration of Competing Interest

The authors declare that they have no known competing financial interests or personal relationships that could have appeared to influence the work reported in this paper.

Data Availability

Data will be made available on request.

Acknowledgement

Appendix A. Supporting information

Supplementary data associated with this article can be found in the online version at doi:10.1016/j.colsurfa.2022.130865.

References

[1] Petrauskas, D.. And Ullah,S. 2015, Manufacture and storage of bitumen, Shell handbook, Sixth Edition, Shell bitumen. (book).
[2] A.G. Marshall, R.P. Rodgers, Petroleomics: chemistry of the underworld, Proc. Natl. Acad. Sci. U.S.A 105 (47) (2008) 18090–18095.
[3] D. Lesueur, The colloidal structure of bitumen: consequences on the rheology and on the mechanisms of bitumen modification, Adv. Colloid Interface Sci. 145 (1–2) (2009) 42–82.
[4] M.H. Schneider, A.B. Andrews, S. Mitra-Kirtley, O.C. Mullins, Asphaltene molecular size by fluorescence correlation spectroscopy, Energy Fuels 21 (2007) 2875–2882.
[5] N.V. Lisitza, D.E. Freed, P.N. Sen, Y.-Q. Song, Study of asphaltene nanoaggregation by nuclear magnetic resonance (NMR), Energy Fuels 23 (2009) 1189–1193.
[6] B. Schuler, G. Meyer, D. Pena, O.C. Mullins, L. Gross, Unraveling the molecular structures of asphaltenes by atomic force microscopy, J. Am. Chem. Soc. 137 (31) (2015) 9870–9876.
[7] B. Schuler, S. Fatayer, G. Meyer, E. Rogel, M. Moir, Y. Zhang, M.R. Harper, A. E. Pomerantz, K.D. Bake, M. Witt, D. Pe.a, J.D. Kushnerick, O.C. Mullins, C. Ovalles, F.G.A. van den Berg, L. Gross, Heavy oil based mixtures of different origins and treatments studied by atomic force microscopy, Energy Fuels 31 (7) (2017) 6856–6861.
[8] F. Handle, M. Harir, J. Füssl, A. Koyun, D. Grossegger, N. Hertkorn, L. Eberhardsteiner, B. Hofko, M. Hospodka, R. Blab, P. Schmitt-Kopplin, H. Grothe, Tracking aging of bitumen and its saturate, aromatic, resin, and asphaltene fractions using high-field fourier transform ion cyclotron resonance mass spectrometry, Energy Fuels 31 (5) (2017) 4771–4779.
[9] W. A. Abdallah, Y. Yang, Raman spectrum of asphaltene, Energy Fuel 26 (2012) 6888–6896.
[10] Kaiser, M.; Klerk, A.; Gary, J.; Handwerk, G. Introduction (chapter), Petroleum refining, Technology and Economics (book), 5th ed.; 2007; pp 1–40.
[11] O. Mullins, The modified yen model†, Energy Fuels 24 (4) (2010) 2179–2207.
[12] (a)(a)S. Ashoori, M. Sharifi, M. Masoumi, M. Salehi, M. Relatsh, SARA Fractions Crude Oil Stab. Egypt. J. Pet. 26 1 2017 209 213.(b) K. Bake, P. Craddock, T. Bolin, W. Abdallah, S. Mitra-Kirtley, A. Andrews, O. Mullins, A. Pomerantz, Structure-solubility relationships in coal, petroleum, and immature source-rock-derived asphaltenes, Energy Fuels 34 (9) (2020) 10825–10836.
[13] J. Putman, R. Moulian, Barr, C. re-Mangote, R. Rodgers, B. Bouyssiere, P. Giusti, A. Marshall, Probing aggregation tendencies in asphaltenes by gel permeation chromatography. Part 1: online inductively coupled plasma mass spectrometry and offline fourier transform ion cyclotron resonance mass spectrometry, Energy Fuels 34 (7) (2020) 8308–8315.
[15] Chen, L.; Bertolini, A.; Dubost, F.; Achourov, V.; Betancourt, S.; Ca.as, J.; Dumont, H.; Pomerantz, A.; Mullins, O. Yen–Mullins Model Applies To Oilfield Reservoirs. Energy & Fuels 2020.
[16] G. Andreatta, N. Bostrom, O.C. Mullins, High-Q ultrasonic determination of the critical nanoaggregate concentration of asphaltenes and the critical micelle concentration of standard surfactants, Langmuir 21 (2005) 2728–2736, 35.
[17] G. Andreatta, C.C. Goncalves, G. Buffin, N. Bostrom, C.M. Quintella, F. Arteaga-Larios, E. Perez, O.C. Mullins, Nanoaggregates and structure- function relations in asphaltenes, Energy Fuels 19 (4) (2005) 1282–1289.
[18] S. Jahromi, A. Khodaii, Effects of nanoclay on rheological properties of bitumen binder, Constr. Build. Mater. 23 (8) (2009) 2894–2904.
[19] H. Yao, Q. Dai, Z. You, M. Ye, Y. Yap, Rheological properties, low-temperature cracking resistance, and optical performance of exfoliated graphite nanoplatelets modified asphalt binder, Constr. Build. Mater. 113 (2016) 988–996.
[20] N. Habib, N. Aun, S. Zoorob, P. Lee, Use of graphene oxide as a bitumen modifier: an innovative process optimization study, Adv. Mater. Res. 1105 (2015) 365–369.
[21] M. Lin, Z. Wang, P. Yang, P. Li, Micro- structure and rheological properties of graphene oxide rubber asphalt, Nanotechnol. Rev. 8 (1) (2019) 227–235.
[22] J. Crucho, L. Picado-Santos, J. Neves, S. Capit.o, A review of nanomaterials' effect on mechanical performance and aging of asphalt mixtures, Appl. Sci. 3657 (2019) 36.
[23] M. Hafeez, N. Ahmad, M. Kamal, J. Rafi, M. Haq, Jamal, S. Zaidi, M. Nasir, Experimental investigation into the structural and functional performance of graphene nano-platelet (GNP)-doped asphalt, Appl. Sci. 9 (4) (2019) 686.
[24] S. Wu, O. Tahri, State-of-art carbon and graphene family nanomaterials for asphalt modification, Road Mater. Pavement Des. 22 (4) (2019) 735–756.
[25] X. Li, Y. Wang, Y. Wu, H. Wang, M. Chen, H. Sun, L. Fan, Properties and modification mechanism of asphalt with graphene as modifier, Constr. Build. Mater. 272 (2021), 121919.
[26] F. Moreno-Navarro, M. Sol-S.nchez, F. Gmiz, M.C. Rubio-Gamez, Mechanical and thermal properties of graphene modified asphalt binders, Constr. Build. Mater. 180 (2018) 265–274.
[27] C. Fang, R. Yu, S. Liu, Y. Li, Nanomaterials applied in asphalt modification: a review, J. Mater. Sci. Technol. 29 (7) (2013) 589–594.
[28] J. Yang, S. Tighe, A review of advances of nanotechnology in asphalt mixtures, Procedia - Soc. Behav. Sci. 96 (2013) 1269–1276.
[29] You, Z., Mills-Beale, J., Foley, J., Roy, S., Odegard, G., Dai, Q. and Goh, Nanoclay-modified asphalt materials: Preparation and characterization. Construction and Building Materials, 25(2), pp.1072–1078.
[30] S. Goh, M. Akin, Z. You, X. Shi, Effect of deicing solutions on the tensile strength of micro- or nano-modified asphalt mixture, Constr. Build. Mater. 25 (1) (2011) 195–200.
[31] M. Khattak, A. Khattab, H. Rizvi, P. Zhang, The impact of carbon nano-fiber modification on asphalt binder rheology, Constr. Build. Mater. 30 (2012) 257–264.
[32] G. Induchoodan, H. Jansson, J. Swenson, Influence of graphene oxide on asphaltene nanoaggregates, Colloids Surf. A: Physicochem. Eng. Asp. 630 (2021), 127614, https://doi.org/10.1016/j.colsurfa.2021.127614.
[33] J. Liu, X. Li, W. Jia, Z. Li, Y. Zhao, S. Ren, Demulsification of crude oil-in-water emulsions driven by graphene oxide nanosheets, Energy Fuels 29 (7) (2015) 4644–4653.
[34] J. Liu, H. Wang, X. Li, W. Jia, Y. Zhao, S. Ren, Recyclable magnetic graphene oxide for rapid and efficient demulsification of crude oil-in-water emulsion, Fuel 189 (1) (2017) 79–87.
[35] T. Lan, H. Zeng, T. Tang, Molecular dynamics study on the mechanism of graphene oxide to destabilize oil/water emulsion, J. Phys. Chem. C 123 (37) (2019) 22989–22999.
[36] H. Wang, J. Liu, H. Xu, Z. Ma, W. Jia, S. Ren, Demulsification of heavy oil-in-water emulsions by reduced graphene oxide nanosheets, RSC Adv. 6 (108) (2016) 106297–106307.
[37] H. Xu, W. Jia, S. Ren, J. Wang, S. Yang, Stable and efficient demulsifier of functional fluorinated graphene for oil separation from emulsified oily wastewaters, J. Taiwan Inst. Chem. Eng. 93 (2018) 492–499.
[38] X. An, T. Simmons, R. Shah, C. Wolfe, K. Lewis, M. Washington, S. Nayak, S. Talapatra, S. Kar, Stable aqueous dispersions of noncovalently functionalized graphene from graphite and their multifunctional high-performance applications, Nano Lett. 10 (11) (2010) 4295–4301.
[39] M. Hinnemo, J. Zhao, P. Ahlberg, C. H.gglund, V. Djurberg, R. Scheicher, S. Zhang, Z. Zhang, On monolayer formation of pyrenebutyric acid on graphene, Langmuir 33 (15) (2017) 3588–3593.
[40] X. Cai, J. Wang, R. Chi, Y. Song, J. Li, Q. Sun, Y. Jia, Direct exfoliation of. graphite into graphene by pyrene-based molecules as molecular-level wedges: a tribological view, Tribol. Lett. 62 (2) (2016) 37.
[41] R. Chen, Y. Zhang, D. Wang, H. Dai, Noncovalent sidewall functionalization of single-walled carbon nanotubes for protein immobilization, J. Am. Chem. Soc. 123 (16) (2001) 3838–3839.

[42] L. Wang, Y. Zhang, A. Wu, G. Wei, Designed graphene-peptide nanocomposites for biosensor applications: a review, Anal. Chim. Acta 985 (2017) 24–40.

[43] M. Zhang, R. Parajuli, D. Mastrogiovanni, B. Dai, P. Lo, W. Cheung, R. Brukh, P. Chiu, T. Zhou, Z. Liu, E. Garfunkel, H. He, Production of graphene sheets by direct dispersion with aromatic healing agents, Small 6 (10) (2010) 1100–1107.

[44] X. Dong, C. Su, W. Zhang, J. Zhao, Q. Ling, W. Huang, P. Chen, L. Li, Ultra-large single layer graphene obtained from solution chemical reduction and its electrical properties, Phys. Chem. Chem. Phys. 12 (9) (2010) 2164.

[45] S. Ghosh, X. An, R. Shah, D. Rawat, B. Dave, S. Kar, S. Talapatra, Effect of 1- pyrene carboxylic-acid functionalization of graphene on its capacitive energy storage, J. Phys. Chem. C 116 (39) (2012) 20688–20693.

[46] X. An, T. Butler, M. Washington, S. Nayak, S. Kar, Optical and sensing properties of 1-pyrenecarboxylic acid-functionalized graphene films laminated on polydimethylsiloxane membranes, ACS Nano 5 (2) (2011) 1003–1011.

[47] L. Goual, A. Firoozabadi, Effect of resins and DBSA on asphaltene precipitation from petroleum fluids, AIChE J. 50 (2) (2004) 470–479.

[48] C. Chang, H. Fogler, Stabilization of asphaltenes in aliphatic solvents using alkylbenzene-derived amphiphiles. 1. Effect of the chemical structure of amphiphiles on asphaltene stabilization, Langmuir 10 (6) (1994) 1749–1757.

[49] L. Goual, M. Sedghi, Role of ion-pair interactions on asphaltene stabilization by alkylbenzenesulfonic acids, J. Colloid Interface Sci. 440 (2015) 23–31.

[50] S. Fakher, M. Ahdaya, M. Elturki, A. Imqam, Critical review of asphaltene properties and factors impacting its stability in crude oil, J. Pet. Explor. Prod. Technol. 10 (3) (2019) 1183–1200.

[51] Y. Larichev, A. Nartova, O. Martyanov, The influence of different organic solvents on the size and shape of asphaltene aggregates studied via small-angle X-ray scattering and scanning tunneling microscopy, Adsorpt. Sci. Technol. 34 (2–3) (2016) 244–257.

[52] G. Gonz.lez, A. Middea, Peptization of asphaltene by various oil soluble amphiphiles, Colloids Surf. 52 (1991) 207–217.

[53] O. Mullins, Review of the molecular structure and aggregation of asphaltenes and petroleomics, SPE J. 13 (01) (2008) 48–57.

[54] Speight, J.Asphaltenes: Fundamentals And Applications By E. Y. Sheu And O. C. Mullins. Plenum Press, New York, 1995; 236 Pages Plus Index. ISBN No. 0–306- 45191–3. Energy & Fuels 1996, 10 (6), 1282–1282.

[55] H. Santos Silva, A. Alfarra, G. Vallverdu, D. B.gu, B. Bouyssiere, I. Baraille, Impact of H-bonds and porphyrins on asphaltene aggregation as revealed by molecular dynamics simulations, Energy Fuels 32 (11) (2018) 11153–11164.

[56] H. Pan, A. Firoozabadi, Thermodynamic micellization model for asphaltene precipitation inhibition, AIChE J. 46 (2) (2000) 416–426.

[57] R. Skartlien, S. Simon, J. Sj.blom, A DPD study of asphaltene aggregation: the role of inhibitor and asphaltene structure in diffusion-limited aggregation, J. Dispers. Sci. Technol. 38 (3) (2016) 440–450.

[58] H. Zeng, Y.-Q. Song, D.L. Johnson, O.C. Mullins, Critical nanoaggregate concentration of asphaltenes by direct-current (DC) eletrical conductivity, Energy Fuels 23 (2009) 1201–1208.

[59] L. Goual, M. Sedghi, H. Zeng, F. Mostowfi, R. McFarlane, O.C. Mullins, On the formation and properties of asphaltene nanoaggregates and clusters by DC- conductivity and centrifugation, Fuel 90 (7) (2011) 2480–2490.

[60] L. Goual, M. Sedghi, F. Mostowfi, R. McFarlane, A.E. Pomerantz, S. Saraji, O. C. Mullins, Cluster of asphaltene nanoaggregates by DC conductivity and centrifugation, Energy Fuels 28 (8) (2014) 5002–5013.

[61] M. Anisimov, I. Yudin, V. Nikitin, G. Nikolaenko, A. Chernoutsan, H. Toulhoat, D. Frot, Y. Briolant, Asphaltene aggregation in hydrocarbon solutions studied by photon correlation spectroscopy, J. Phys. Chem. 99 (23) (1995) 9576–9580.

[62] S. Hashmi, K. Zhong, A. Firoozabadi, Acid–base chemistry enables reversible colloid-to-solution transition of asphaltenes in non-polar systems, Soft Matter 8 (33) (2012) 8778.

[63] C. Chang, H. Fogler, Stabilization of asphaltenes in aliphatic solvents using alkylbenzene-derived amphiphiles. 1. Effect of the chemical structure of amphiphiles on asphaltene stabilization, Langmuir 10 (6) (1994) 1749–1757.

[64] B. Jiang, R. Zhang, N. Yang, L. Zhang, Y. Sun, C. Jian, L. Liu, Z. Xu, Molecular mechanisms of suppressing asphaltene aggregation and flocculation by dodecylbenzenesulfonic acid probed by molecular dynamics simulations, Energy Fuels 33 (6) (2019) 5067–5080.

[65] T. Al-Sahhaf, M. Fahim, A. Elkilani, Retardation of asphaltene precipitation by addition of toluene, resins, deasphalted oil and surfactants, Fluid Phase Equilibria 194–197 (2002) 1045–1057.

[66] M. Alhreez, D. Wen, Molecular structure characterization of asphaltene in the presence of inhibitors with nanoemulsions, RSC Adv. 9 (34) (2019) 19560–19570.

[67] R. Xiong, J. Guo, W. Kiyingi, H. Feng, T. Sun, X. Yang, Q. Li, Method for judging the stability of asphaltenes in crude oil, Omega 5 (34) (2020) 21420–21427.

[68] M. Nategh, H. Mahdiyar, M. Malayeri, M. Binazadeh, Impact of asphaltene surface energy on stability of asphaltene–toluene system: a parametric study, Langmuir 34 (46) (2018) 13845–13854.

[69] D. Mitchell, J. Speight, The solubility of asphaltenes in hydrocarbon solvents, Fuel 52 (2) (1973) 149–152.

[70] I. Wiehe, H. Yarranton, K. Akbarzadeh, P. Rahimi, A. Teclemariam, The paradox of asphaltene precipitation with normal paraffins, Energy Fuels 19 (4) (2005) 1261–1267.

[71] Wang, J., 2000. Predicting asphaltene flocculation in crude oils. New Mexico: New Mexico Institute of Mining and Technology, (PhD thesis).

[72] N. Haji-Akbari, P. Masirisuk, M. Hoepfner, H. Fogler, A unified model for aggregation of asphaltenes, Energy Fuels 27 (5) (2013) 2497–2505.

[73] J. Calles, J. Dufour, J. Marugán, J. Peña, R. Giménez-Aguirre, D. Merino-García, Properties of asphaltenes precipitated with different n-alkanes. a study to assess the most representative species for modeling, Energy Fuels 22 (2) (2007) 763–769.

[74] Haji Akbari Balou, N, Destabilization and Aggregation Kinetics of Asphaltenes, The University of Michigan, (PhD thesis), Michigan, 2014.

[75] R. Nguele, A. Mbouopda Poupi, G. Anombogo, O. Alade, H. Saibi, Influence of asphaltene structural parameters on solubility, Fuel 311 (2022), 122559.

[76] O. Mullins, A. Pomerantz, J. Zuo, C. Dong, Downhole fluid analysis and asphaltene science for petroleum reservoir evaluation, Annu. Rev. Chem. Biomol. Eng. 5 (1) (2014) 325–345, https://doi.org/10.1146/annurev-chembioeng-060713-035923.

[77] https://xgsciences.com/wp-content/uploads/2018/10/xGnP-M-Grade-XG-Sciences.pdf.

[78] V. Hemanth Kumar, S. Suresha, Investigation of aging effect on asphalt binders using thin film and rolling thin film oven test, Adv. Civ. Eng. Mater., 8 (1) (2019), Article 20190119.

[79] E. Rogel, C. Ovalles, M. Moir, J. Schabron, Determination of asphaltenes in crude oil and petroleum products by the on column precipitation method, Energy Fuels 23 (9) (2009) 4515–4521, https://doi.org/10.1021/ef900358q.

[80] E. Johansson, L. Nyborg, XPS study of carboxylic acid layers on oxidized metals with reference to particulate materials, Surf. Interface Anal. 35 (4) (2003) 375–381, https://doi.org/10.1002/sia.1537.

[81] E. Chailleux, C. Queffélec, I. Borghol, F. Farcas, S. Marceau, B. Bujoli, Bitumen fractionation: contribution of the individual fractions to the mechanical behavior of road binders, Constr. Build. Mater. 271 (2021), 121528.

[82] P. Apostolidis, M. Elwardany, L. Porot, S. Vansteenkiste, E. Chailleux, Glass transitions in bituminous binders, Mater. Struct. 54 (2021), https://doi.org/10.1617/s11527-021-01726-6.

[83] D. Santos, M. Amaral, E. Filho, R. Dourado, J. Coutinho, G. Borges, et al., Revisiting the methodology for asphaltenes precipitation, J. Pet. Sci. Eng. 178 (2019) 778–786, https://doi.org/10.1016/j.petrol.2019.03.074.

[84] H. Vignisdottir, B. Ebrahimi, G. Booto, R. O'Born, H. Bratteb, H. Wallbaum, R. Bohne, Life cycle assessment of winter road maintenance, Int. J. Life Cycle Assess. 25 (3) (2019) 646–661, https://doi.org/10.1007/s11367-019-01682-y.

[85] V. Mohan, K. Lau, D. Hui, D. Bhattacharyya, Graphene-based materials and their composites: a review on production, applications and product limitations, Compos. Part B: Eng. 142 (2018) 200–220, https://doi.org/10.1016/j.compositesb.2018.01.013.